Optimal Configuration Strategy of Electricity–Hydrogen Coupled Rural Microgrid Considering Long-Term Hydrogen Storage Characteristics

Xiaodong Yuan[1], Huiyu Miao[1], Mingshen Wang[1], Ai Du[2], Xuefei Li[2], Yi Pan[1], Fei Zeng[1]
[1]Jiangsu Electric Power Research Institute Company Ltd., Nanjing 211100, China
[2]School of Electrical Engineering, Southeast University, Nanjing 210096, China
Corresponding author: Xiaodong Yuan (e-mail: 220243136@seu.edu.cn).

ABSTRACT The limited flexibility of rural microgrids in accommodating long-term renewable energy fluctuations poses a major challenge to achieving low-carbon and cost-effective operation. To address this issue, an optimal configuration strategy for an electricity–hydrogen coupled rural microgrid (EH-RM) system is developed, considering the long-term operational characteristics of hydrogen storage. Firstly, detailed models of key energy conversion and storage devices, including electrolyzers, fuel cells, combined heat and power (CHP) units, and hydrogen storage tanks, are established to capture multi-energy coupling relationships among electricity, heat, gas, and hydrogen. Then, a bilevel optimization framework is proposed, where the upper-level capacity configuration model minimizes the annualized total cost, and the lower-level scheduling model minimizes daily operating cost under multi-energy balance constraints. Subsequently, a Benders decomposition–based algorithm is employed to decouple capacity planning and operational scheduling, iteratively generating feasibility and optimality cuts to ensure convergence and computational efficiency. Finally, case study results show that the proposed bilevel configuration model effectively reduces the total system cost and carbon emissions in rural applications, demonstrating its economic efficiency and low-carbon advantages for rural integrated scenarios.

INDEX TERMS electro-hydrogen coupled, long-term hydrogen storage, bilevel configuration optimization, Benders decomposition, rural microgrid

I. INTRODUCTION

DRIVEN by the worldwide momentum for low-carbon microgrids, transitioning to a clean energy mix dominated by renewables is now imperative [1]. Conversely, the variable and uncertain characteristics of sources like wind and solar significantly complicate the maintenance of system flexibility and threaten the stability margins of electrical networks [2].

To address the volatility and uncertainty of PV generation, hydrogen energy, with its long-duration, low-carbon, and clean storage characteristics, mitigates the curtailment of renewable generation [3]. Accurate sizing of hydrogen storage is a prerequisite for ensuring the economic and stable dispatch of integrated energy systems [4]. Focusing on campus scenarios, Reference [5] proposed an integrated system equipped with hybrid hydrogen and thermal storage. By applying a bilevel configuration strategy, the study quantified the economic advantages of the electricity–gas–cooling–heating coordination. Reference [6] established a comprehensive energy system with hydrogen storage for an industrial park. By employing a Stackelberg game model to align the interests of the operator with the user side, the study verified the role of hydrogen storage in improving energy balance. Reference [7] proposed a bilevel mixed-integer linear programming model for a regional integrated electricity and hydrogen energy system. By optimizing equipment capacity in conjunction with wind power, solar thermal, and geothermal resources, the model achieves synergy between renewable energy penetration and hydrogen energy development. Reference [8] introduced a novel configuration method considering hybrid energy storage. By performing annualized time-series simulations to optimize the capacities of the critical equipment of the system, the curtailment rate of renewable energy utilization was decreased, with the investment cost reduced. Reference [9] designed a cascaded hydrogen storage system and employed the NSGA-II algorithm to optimize the pressure levels and capacity configurations. The results showed that this approach effectively reduced the overall system energy consumption and demonstrated the advantages of multi-stage hydrogen storage under complex operational scenarios. Reference [10] developed a renewable full-chain hydrogen energy system, which achieved a self-sufficient zero-carbon energy solution. Reference [11] optimized the configuration of a green hydrogen system, achieving a levelized cost of hydrogen below 10 USD/kg, thereby providing a feasible technological pathway for hydrogen commercialization. However, most existing studies focus on specific industrial park scenarios, with limited attention to the unique characteristics of rural distributed energy systems, highlighting the need for customized models adapted to local resource conditions.

The rational planning of hydrogen storage plays a vital role in mitigating seasonal energy fluctuations. Reference [12] proposed a futures-based carbon trading mechanism integrated with seasonal hydrogen storage, effectively smoothing the net load peaks and valleys. Reference [13] established a bilevel robust-stochastic optimization model, employing a coordinated approach using column-and-constraint generation alongside particle swarm optimization to coordinate source–load uncertainties and seasonal storage, thereby enhancing wind power utilization and system economic performance. These studies provide valuable theoretical support for addressing the seasonal energy supply–demand imbalance.

Hydrogen storage enhances system flexibility by acting as a multi-energy conversion hub that bridges different energy forms [14]. Reference [15] proposed a hybrid optimization method combining the Particle Swarm Optimization and Maximum Matrix Method for an integrated energy park coupled with hydrogen storage, achieving optimal system capacity configuration. Reference [16] integrated solar thermal collectors with hydrogen storage, breaking the rigid coupling of combined heat and power systems and improving overall energy supply economics by 6.2%. Reference [17] designed a solar–hydrogen–organic Rankine cycle hybrid system, achieving a daily electricity output of 208.5 kWh and hydrogen production of 1.1 kg, demonstrating the technical potential of multi-energy complementarity. Reference [18] optimized the coordination between electrolyzers and hydrogen fuel cells, reducing hydrogen production costs by 15% through waste heat recovery. However, in rural regions, in addition to solar and hydrogen resources, biomass energy is also abundant. Current studies rarely address how to efficiently integrate biomass energy with other energy forms, highlighting a gap in research on comprehensive multi-energy utilization in rural energy systems.

Reference [19] proposed an adaptive NSGA-II algorithm that improves the crossover and mutation rates; the case study showed that the loss-of-load rate decreased to 0.065, and the convergence speed improved by 20% compared with traditional algorithms. Reference [20] applied the Karush–Kuhn–Tucker conditions to transform a bilevel optimization problem into a single-level linear formulation, demonstrating that hydrogen storage configuration reduces user energy purchase costs by 9.3%. Reference [21] developed an energy framework integrating renewable power generation, power-to-hydrogen, and energy storage, constructing a multi-objective configuration model that achieved strong economic and low-carbon performance in case studies. Reference [22] proposed a dual-stage architecture integrating diverse decision strategies, combining NSGA-II and the entropy weight method to determine the optimal capacity of PV, battery, and hydrogen storage systems, improving power supply reliability to 48.9%. Reference [23] constructed a multi-objective optimization framework to analyze the synergistic effects between hydrogen storage and batteries, with the minimum LCOE reaching 0.446 USD/kWh, providing theoretical support for long-duration energy storage planning. In rural integrated energy system configuration, it is necessary not only to consider source–load uncertainty but also the uncertainties arising from policy and market mechanisms. Integrating carbon trading mechanisms can enhance the economic benefits of hydrogen storage. Reference [24] developed a stochastic optimization model incorporating carbon capture and power-to-hydrogen processes, verifying the economic feasibility of low-carbon and flexible system operation. A carbon tax sensitivity analysis was conducted to provide valuable insights for policy design. Reference [25] proposed a hybrid energy storage configuration model considering tiered carbon trading and demand response, optimized using a NSGA-II. The results showed that the load peak–valley difference was reduced by 15%, while carbon tax costs decreased by 1.5%.

In summary, existing studies have achieved remarkable progress in urban and industrial contexts; however, research on optimal configuration considering the long-term operational characteristics of hydrogen storage in rural scenarios remains limited. To address this gap, this paper develops a bilevel optimization model for electricity–hydrogen coupled systems that incorporates the long-term operation of hydrogen storage. Through the coordinated design of capacity planning and operational scheduling, the proposed model achieves global optimization in terms of economic efficiency, flexibility, and carbon reduction, providing theoretical and engineering references for the sustainable planning of rural energy systems.

II. STRUCTURE OF EH-RM

The EH-RM system constructed in this paper consists of four subsystems: power supply, heat supply, gas supply, and hydrogen supply. On this basis, mathematical models are developed for the four subsystems, including electricity, heat, gas, and hydrogen. The power supply section comprises photovoltaic, waste-to-power, and CHP units; the heat supply section utilizes waste heat from CHP and thermal storage devices to meet heat loads; the gas supply section primarily relies on biomass biogas and can interact with external gas networks; the hydrogen supply section enables the production, storage, and utilization of hydrogen through electrolytic hydrogen production and fuel cells.

On this basis, mathematical models are established for the four subsystems of electricity, heat, gas, and hydrogen to describe their energy balance relationships, conversion efficiencies, and operational constraints, thereby enabling the coordinated optimization and operational analysis of the EH-RM system.

A. SOURCE-SIDE MODEL

The distributed photovoltaic generation model is constructed:

$$P_{\mathrm{PV}}(t)=P_{\mathrm{STC}}\frac{G_{\mathrm{ING}}(t)}{G_{\mathrm{STC}}}\left[1+k_{\mathrm{PV}}\left(T_c(t)-T_r\right)\right] \tag{1}$$

where $P_{\mathrm{PV}}(t)$ is the real-time power generation; P_{STC} is the nominal rated capacity; $G_{\mathrm{ING}}(t)$ and G_{STC} correspond to the incident solar radiation and the standard irradiance, respectively; k_{PV} is the temperature coefficient; $T_c(t)$ and T_r stand for the operating temperature and reference temperature.

The waste-to-energy supply model is shown:

$$H_{\mathrm{WI}}(t)=W_{\mathrm{gar}}(t)\alpha_{\mathrm{WI}}\beta_{\mathrm{WI}}q_{\mathrm{WI}}\eta_{\mathrm{WI}} \tag{2}$$

$$H_{\mathrm{WG}}(t)=W_{\mathrm{gar}}(t)\alpha_{\mathrm{WG}}q_{\mathrm{WG}}\eta_{\mathrm{WG}} \tag{3}$$

$$H_{\mathrm{gar}}(t)=H_{\mathrm{WI}}(t)+H_{\mathrm{WG}}(t) \tag{4}$$

$$P_{\mathrm{gar}}(t)=\left(H_{\mathrm{WI}}(t)+H_{\mathrm{WG}}(t)\right)\eta_{\mathrm{WHB}}(1-\eta_{\mathrm{aux}}) \tag{5}$$

where $H_{\mathrm{WI}}(t)$ and $H_{\mathrm{WG}}(t)$ denote the thermal yields from waste incineration and gasification, respectively; $H_{\mathrm{gar}}(t)$ is the total thermal energy produced from waste; $P_{\mathrm{gar}}(t)$ denotes the electricity generated from waste; $W_{\mathrm{gar}}(t)$ is the amount of waste processed at time t; α_{WI} and α_{WG} are the proportions of combustible and gasifiable components in the municipal solid waste, respectively; β_{WI} is the proportion of combustible waste remaining after leachate removal from the storage pit; q_{WI} and q_{WG} are the lower heating values of combustible and gasifiable waste, respectively; η_{WI}, η_{WG}, η_{WHB}, and η_{aux} denote the efficiencies of the incinerator, pyrolysis gasifier, steam turbine, and auxiliary power consumption, respectively.

The biomass resources in rural areas are converted into biogas through anaerobic fermentation, and the required thermal power of the digester is affected by the reaction temperature, heat dissipation, and digester volume.

$$H_{\mathrm{BD}}(t)=\left(T_z(t+1)-T_z(t)\right)V_B c_m \rho_m+H_{\mathrm{loss}}(t) \tag{6}$$

$$\begin{aligned}H_{\mathrm{loss}}(t)=&\,c_m M_{\mathrm{BD}}(t)\left(T_z(t)-T_e\right)\\&+k_o A_o\left(T_z(t)-T_e\right)\end{aligned} \tag{7}$$

where $H_{\mathrm{BD}}(t)$ is the heating power input; $H_{\mathrm{loss}}(t)$ is the heat loss power of the digester; the physical parameters V_B, c_m, and ρ_m stand for the digester volume, feedstock specific heat, and density, respectively; $M_{\mathrm{BD}}(t)$ is the quantity of organic waste fed into the system; A_o and k_o refer to the internal heat transfer area and coefficient; T_e is the external temperature.

The biogas production model is expressed as:

$$V_{\mathrm{BD}}(t)=\alpha_{\mathrm{BD}}M_{\mathrm{BD}}(t)+\beta_{\mathrm{BD}}H_{\mathrm{BD}}(t) \tag{8}$$

where α_{BD} is the specific biogas yield based on organic mass, and β_{BD} is the coefficient relative to the thermal energy supply.

The natural gas power obtained after biogas purification is expressed as:

$$G_{\mathrm{BD}}(t)=V_{\mathrm{BD}}(t)\eta_{\mathrm{B2G}}q_{\mathrm{CH4}} \tag{9}$$

where $G_{\mathrm{BD}}(t)$ is the natural gas from purified biogas; η_{B2G} is the purification efficiency coefficient for converting biogas into natural gas; q_{CH4} is the heating value of natural gas.

B. ENERGY CONVERSION EQUIPMENT MODEL

The hydrogen production model of the electrolyzer is:

$$m_{\mathrm{EL}}(t)=\frac{\eta_{\mathrm{EL,H2}}P_{\mathrm{EL}}(t)}{q_{\mathrm{H}}} \tag{10}$$

where $m_{\mathrm{EL}}(t)$ is the mass of hydrogen output; $\eta_{\mathrm{EL,H2}}$ is the hydrogen conversion efficiency; $P_{\mathrm{EL}}(t)$ is the electricity consumption of the electrolyzer; q_{H} is the lower heating value of hydrogen.

The heat recovery model of the electrolyzer is expressed as:

$$H_{\mathrm{EL}}(t)=\eta_{\mathrm{EL,h}}\left(1-\eta_{\mathrm{EL,H2}}\right)P_{\mathrm{EL}}(t) \tag{11}$$

where $H_{\mathrm{EL}}(t)$ is the waste heat captured from the electrolysis process; $\eta_{\mathrm{EL,h}}$ is the recovery efficiency of the thermal management system.

The model of the hydrogen fuel cell is as follows:

$$P_{\mathrm{FC}}(t)=\eta_{\mathrm{FC,e}}m_{\mathrm{FC}}(t)q_{\mathrm{H}} \tag{12}$$

where $P_{\mathrm{FC}}(t)$ is the electric power output of the hydrogen fuel cell; $\eta_{\mathrm{FC,e}}$ is the electrical conversion efficiency; $m_{\mathrm{FC}}(t)$ is the consumed hydrogen mass.

The heat recovery model of the hydrogen fuel cell is as shown:

$$H_{\mathrm{FC}}(t)=\eta_{\mathrm{FC,h}}m_{\mathrm{FC}}(t)q_{\mathrm{H}} \tag{13}$$

where $H_{\mathrm{FC}}(t)$ is the thermal energy yield from the hydrogen fuel cell; $\eta_{\mathrm{FC,h}}$ is the heat production coefficient.

The power and heat generation models of the CHP unit are equivalently represented as:

$$\begin{aligned}P_{\mathrm{CHP}}(t)&=\eta_{\mathrm{CHP}}G_{\mathrm{CHP}}(t),\\H_{\mathrm{CHP}}(t)&=\eta_{\mathrm{CHP}}\alpha_{\mathrm{CHP}}G_{\mathrm{CHP}}(t)\end{aligned} \tag{14}$$

where $G_{\mathrm{CHP}}(t)$, $P_{\mathrm{CHP}}(t)$, and $H_{\mathrm{CHP}}(t)$ represent the input gas power, electricity output, and heat output of the CHP unit, respectively; η_{CHP} and α_{CHP} represent the electrical conversion efficiency and the conversion ratio, respectively.

C. ENERGY STORAGE EQUIPMENT MODEL

The temporal energy evolution of the BESS during charge and discharge cycles is described by:

$$\begin{aligned}S_{\mathrm{ES}}(t+1)=&\,(1-\sigma_{\mathrm{ES}}\Delta t)S_{\mathrm{ES}}(t)\\&+\left(\eta_{\mathrm{ES}}P_{\mathrm{ES,ch}}(t)-\frac{P_{\mathrm{ES,dis}}(t)}{\eta_{\mathrm{ES}}}\right)\Delta t\end{aligned} \tag{15}$$

where $S_{\mathrm{ES}}(t)$ denotes the instantaneous energy state of the battery; σ_{ES} is the battery self-discharge rate; η_{ES} is the round-trip efficiency; $P_{\mathrm{ES,ch}}(t)$ and $P_{\mathrm{ES,dis}}(t)$ denote the power absorption and power injection rates, respectively.

The upper and lower limit constraints of energy storage must be satisfied:

$$\alpha_{\mathrm{ES,min}} S_{\mathrm{ES,cap}} \leq S_{\mathrm{ES}}(t) \leq \alpha_{\mathrm{ES,max}} S_{\mathrm{ES,cap}} \tag{16}$$

where $S_{\mathrm{ES,cap}}$ is the maximum capacity of the battery; $\alpha_{\mathrm{ES,min}}$ and $\alpha_{\mathrm{ES,max}}$ represent the minimum and maximum SOC (state of charge) ratios of the battery, respectively.

Since battery cannot charge and discharge simultaneously, the charging and discharging power must satisfy the following constraint:

$$0 \leq P_{\mathrm{ES,ch}}(t) \leq z_{\mathrm{ES,ch}}(t) \beta_{\mathrm{ES,ch}} S_{\mathrm{ES,cap}} \tag{17}$$

$$0 \leq P_{\mathrm{ES,dis}}(t) \leq z_{\mathrm{ES,dis}}(t) \beta_{\mathrm{ES,dis}} S_{\mathrm{ES,cap}} \tag{18}$$

$$z_{\mathrm{ES,ch}}(t) + z_{\mathrm{ES,dis}}(t) \leq 1 \tag{19}$$

where $z_{\mathrm{ES,ch}}(t)$ and $z_{\mathrm{ES,dis}}(t)$ are the binary decision variables that determine the charging and discharging modes, respectively; $\beta_{\mathrm{ES,ch}}$ denotes the ratio of maximum charging power to the battery capacity, representing the fastest allowable charging rate under rated conditions; $\beta_{\mathrm{ES,dis}}$ is the maximum discharging rate.

To facilitate periodic control of the system, total energy variation of the battery over the scheduling period is constrained to maintain balance:

$$\sum_{t=1}^{T} \left(\eta_{\mathrm{ES,ch}} P_{\mathrm{ES,ch}}(t) - \frac{P_{\mathrm{ES,dis}}(t)}{\eta_{\mathrm{ES,dis}}} \right) = 0 \tag{20}$$

The state model of the heat storage tank is:

$$S_{\mathrm{HS}}(t+1) = (1 - \sigma_{\mathrm{HS}} \Delta t) S_{\mathrm{HS}}(t) + \left(\eta_{\mathrm{HS}} H_{\mathrm{HS,ch}}(t) - \frac{H_{\mathrm{HS,dis}}(t)}{\eta_{\mathrm{HS}}} \right) \Delta t \tag{21}$$

where $S_{\mathrm{HS}}(t)$ represents the accumulated thermal energy; σ_{HS} is the static heat loss factor; η_{HS} is the operational efficiency; $H_{\mathrm{HS,ch}}(t)$ and $H_{\mathrm{HS,dis}}(t)$ denote the input and output heat power, respectively.

The thermal energy stored in the tank must obey the limit constraints:

$$\alpha_{\mathrm{HS,min}} S_{\mathrm{HS,cap}} \leq S_{\mathrm{HS}}(t) \leq \alpha_{\mathrm{HS,max}} S_{\mathrm{HS,cap}} \tag{22}$$

where $S_{\mathrm{HS,cap}}$ denotes the rated thermal capacity; $\alpha_{\mathrm{HS,min}}$ and $\alpha_{\mathrm{HS,max}}$ represent the lower and upper bounds for the tank SOC, respectively.

Since the mutual exclusivity of the heat charging and discharging processes, the operating thermal power must satisfy the following constraint:

$$0 \leq P_{\mathrm{HS,ch}}(t) \leq z_{\mathrm{HS,ch}}(t) \beta_{\mathrm{HS,ch}} S_{\mathrm{HS,cap}} \tag{23}$$

$$0 \leq P_{\mathrm{HS,dis}}(t) \leq z_{\mathrm{HS,dis}}(t) \beta_{\mathrm{HS,dis}} S_{\mathrm{HS,cap}} \tag{24}$$

$$z_{\mathrm{HS,ch}}(t) + z_{\mathrm{HS,dis}}(t) \leq 1 \tag{25}$$

where $z_{\mathrm{HS,ch}}(t)$ and $z_{\mathrm{HS,dis}}(t)$ are Boolean decision variables determining the active heat storage or release modes; $\beta_{\mathrm{HS,ch}}$ and $\beta_{\mathrm{HS,dis}}$ represent the normalized maximum power coefficients regarding heat storage and release.

To facilitate periodic control of the tank, the total energy variation within the scheduling period is constrained to maintain balance:

$$\sum_{t=1}^{T} \left(\eta_{\mathrm{HS,ch}} H_{\mathrm{HS,ch}}(t) - \frac{H_{\mathrm{HS,dis}}(t)}{\eta_{\mathrm{HS,dis}}} \right) = 0 \tag{26}$$

The operating model of the hydrogen storage tank is as follows:

$$S_{\mathrm{H2S}}(t+1) = (1 - \sigma_{\mathrm{H2S}} \Delta t) S_{\mathrm{H2S}}(t) + \left(\eta_{\mathrm{H2S}} m_{\mathrm{H2S,ch}}(t) - \frac{m_{\mathrm{H2S,dis}}(t)}{\eta_{\mathrm{H2S}}} \right) \Delta t \tag{27}$$

where $S_{\mathrm{H2S}}(t)$ is the mass state of the stored hydrogen; σ_{H2S} is the self-loss rate of the stored hydrogen; η_{H2S} is the storage efficiency; $m_{\mathrm{H2S,ch}}(t)$ and $m_{\mathrm{H2S,dis}}(t)$ are the mass inflow and outflow quantities, respectively.

The hydrogen stored in the tank must also satisfy the energy limit constraints:

$$\alpha_{\mathrm{H2S,min}} S_{\mathrm{H2S,cap}} \leq S_{\mathrm{H2S}}(t) \leq \alpha_{\mathrm{H2S,max}} S_{\mathrm{H2S,cap}} \tag{28}$$

where $S_{\mathrm{H2S,cap}}$ is the maximum capacity of the storage tank; $\alpha_{\mathrm{H2S,min}}$ and $\alpha_{\mathrm{H2S,max}}$ represent the bound of energy storage ratios of the tank, respectively.

Since the hydrogen storage tank cannot charge and discharge simultaneously, the hydrogen flow must satisfy the following constraint:

$$0 \leq P_{\mathrm{H2S,ch}}(t) \leq z_{\mathrm{H2S,ch}}(t) \beta_{\mathrm{H2S,ch}} S_{\mathrm{H2S,cap}} \tag{29}$$

$$0 \leq P_{\mathrm{H2S,dis}}(t) \leq z_{\mathrm{H2S,dis}}(t) \beta_{\mathrm{H2S,dis}} S_{\mathrm{H2S,cap}} \tag{30}$$

$$z_{\mathrm{H2S,ch}}(t) + z_{\mathrm{H2S,dis}}(t) \leq 1 \tag{31}$$

where $z_{\mathrm{H2S,ch}}(t)$ and $z_{\mathrm{H2S,dis}}(t)$ are Boolean decision variables that govern the hydrogen injection and extraction modes, respectively; $\beta_{\mathrm{H2S,ch}}$ and $\beta_{\mathrm{H2S,dis}}$ refer to maximum hydrogen charging and discharging ratio.

III. BILEVEL OPTIMAL CONFIGURATION OF ELECTRICITY–HYDROGEN COUPLED SYSTEMS WITH LONG-TERM HYDROGEN STORAGE

To address the coupling between long-term capacity investment planning and short-term operational scheduling, a bilevel optimization framework is proposed, enabling interactive decision-making between the capacity configuration layer and the operational scheduling layer to achieve global optimality. The upper layer constructs the configuration model to determine the optimal types and capacities of system equipment, while the lower layer focuses on operational scheduling model to determine the optimal operation strategies for the selected equipment. The configuration model framework is shown in Figure 1.

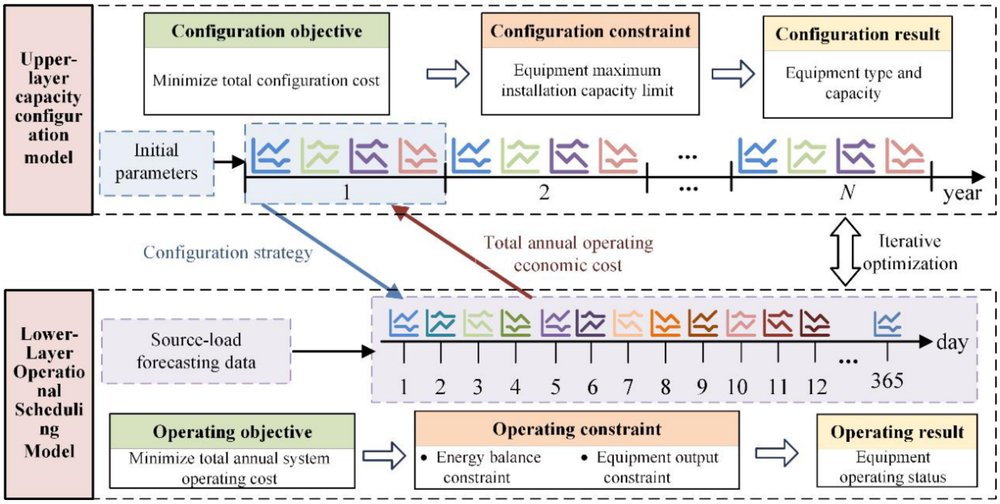

FIGURE 1. Bilevel Configuration Optimization Model Framework

A. UPPER-LAYER CAPACITY CONFIGURATION MODEL

The upper-layer capacity configuration model takes the minimization of the annualized total cost over the system life cycle as its objective. The life-cycle annualized total cost consists of four components: annualized investment cost C_{inv}, operation cost C_{op}, decommissioning cost C_{scrap}, and loss cost C_{loss}.

$$\min C = C_{\text{inv}} + C_{\text{op}} + C_{\text{scrap}} + C_{\text{loss}} \tag{32}$$

The annualized investment cost C_{inv} refers to the total equipment investment cost converted into an equivalent annual cost using the capital recovery factor. The conversion model can be expressed as:

$$C_{\text{inv}} = \frac{r(1+r)^y}{(1+r)^y - 1} \sum_{i}^{X} \mu_i S_i \tag{33}$$

where y represents the life cycle of the equipment; μ_i denotes the unit capacity cost of the equipment type i; r denotes the discount rate; S_i represents the installed capacity; X represents the set of equipment subject to capacity configuration in the system, including waste-to-energy units, biogas fermentation units, electrolyzers, hydrogen fuel cells, CHP units, batteries, heat and hydrogen storage tanks.

The operation cost C_{op} represents the total annual operating expenses of all equipment in the system, which includes the annual operation and maintenance cost (O&M Cost) C_{om}, energy purchase cost C_{buy}, carbon trading cost C_{CO2}, waste treatment subsidy C_{waste}, and energy sales revenue C_{sell}:

$$\begin{aligned} C_{\text{op}} = \sum_{k=1}^{s} N_r p_k \big(& C_{\text{om},k} + C_{\text{buy},k} + C_{\text{CO2},k} \\ & - C_{\text{waste},k} - C_{\text{sell},k} \big) \end{aligned} \tag{34}$$

where s denotes the number of typical days in a year; p_k is the weighting factor assigned to the k-th scenario; N_r represents the annual number of operating days.

The decommissioning cost C_{scrap} refers to the disposal expenses incurred when equipment in the system reaches the end of its service life, becomes technologically obsolete, or fails. To simplify the calculation, it is set as 3% of the initial investment cost.

The loss cost C_{loss} represents the economic loss caused by energy dissipation during conversion, transmission, and storage processes. To simplify the calculation, it is set as 5% of the energy purchase cost.

The constraints of the configuration model mainly consider the limitation of equipment installation capacity:

$$0 \leq S_i \leq S_{i,\max} \tag{35}$$

where S_i is the maximum allowable installation capacity of equipment type i.

B. LOWER-LAYER OPERATIONAL SCHEDULING MODEL

In the lower-layer operational scheduling model, the objective is to minimize annual operating system cost:

$$\begin{aligned} \min C_{\text{op}} = \sum_{k=1}^{s} N_r p_k \big(& C_{\text{om},k} + C_{\text{buy},k} + C_{\text{CO2},k} \\ & - C_{\text{waste},k} - C_{\text{sell},k} \big) \end{aligned} \tag{36}$$

The constraints of the lower-layer operational scheduling model include the energy balance constraints, equipment output upper and lower limits, energy purchase constraints, and energy storage equipment constraints.

The electric power balance constraint is expressed as:

$$\begin{aligned} & P_{\text{buy}}(r,t) + P_{\text{PV}}(r,t) + P_{\text{gar}}(r,t) + P_{\text{FC}}(r,t) \\ & \quad + P_{\text{CHP}}(r,t) + P_{\text{ES,dis}}(r,t) \\ & = P_{\text{EL}}(r,t) + P_{\text{EB}}(r,t) + P_{\text{ES,ch}}(r,t) + P_{\text{L}}(r,t) \end{aligned} \tag{37}$$

where $P_{\text{L}}(r,t)$ represents the electrical load of the system on operating day r.

The heat power balance constraint is expressed as:

$$\begin{aligned} &H_{\mathrm{gar}}(r,t)+H_{\mathrm{CHP}}(r,t)+H_{\mathrm{EL}}(r,t)+H_{\mathrm{FC}}(r,t)\\ &\quad+H_{\mathrm{EB}}(r,t)+H_{\mathrm{HS,dis}}(r,t)\\ &=H_{\mathrm{BD}}(r,t)+H_{\mathrm{HS,ch}}(r,t)+H_{\mathrm{L}}(r,t) \end{aligned} \tag{38}$$

where $H_{\mathrm{L}}(r,t)$ represents the thermal load of the system on operating day r.

Natural Gas Balance Constraint is:

$$G_{\mathrm{buy}}(r,t)+G_{\mathrm{BD}}(r,t)=G_{\mathrm{CHP}}(r,t)+G_{\mathrm{L}}(r,t) \tag{39}$$

where $G_{\mathrm{L}}(r,t)$ represents the natural gas load of the system on operating day r at time period t.

Hydrogen Energy Balance Constraint is expressed as:

$$\begin{aligned} m_{\mathrm{EL}}(r,t)+m_{\mathrm{H2S,dis}}(r,t)=m_{\mathrm{FC}}(r,t)+m_{\mathrm{sell}}(r,t)\\ +m_{\mathrm{H2S,ch}}(r,t)+m_{\mathrm{L}}(r,t) \end{aligned} \tag{40}$$

where $m_{\mathrm{L}}(r,t)$ is the hydrogen load on operating day r.

The system's energy purchase constraints ensure that the amounts of electricity and natural gas purchased remain within permissible ranges, thereby maintaining the stability and economic efficiency of system operation.

$$P_{\mathrm{buy,min}}\le P_{\mathrm{buy}}(t)\le P_{\mathrm{buy,max}} \tag{41}$$

$$G_{\mathrm{buy,min}}\le G_{\mathrm{buy}}(r,t)\le G_{\mathrm{buy,max}} \tag{42}$$

The output of each device in the system is constrained by its performance characteristics and system requirements, and is typically subject to upper and lower output limits as well as ramping rate constraints.

$$P_{i,\mathrm{min}}\le P_i(r,t)\le P_{i,\mathrm{max}} \tag{43}$$

$$R_{i,\mathrm{down}}\le P_i(r,t)-P_i(r,t-1)\le R_{i,\mathrm{up}} \tag{44}$$

The power constraints of the battery, the thermal energy storage tank, and the hydrogen storage tank have already been discussed in Section 2.3.

C. BILEVEL MODEL SOLUTION METHOD

To address the potential convergence issues that may arise when directly solving the bilevel configuration optimization model, it is necessary to adopt an efficient solution method. Given the inherent hierarchical distinction between the upper-level sizing and lower-level operational subproblems, the proposed electricity-hydrogen planning framework is amenable to the Benders Decomposition algorithm. This approach is particularly effective as the formulated model represents a Mixed-Integer Linear Programming (MILP) problem. This approach effectively decouples the equipment capacity planning from the operational strategy optimization. By iteratively generating and adding Benders cuts, the algorithm gradually approximates the global optimal solution, thereby avoiding direct computation of a high-dimensional nonconvex problem. Accordingly, the bilevel model is efficiently solved using the Benders decomposition method in combination with the Gurobi optimizer.

The bilevel configuration model is formulated as the following MILP:

$$\begin{aligned} \min\quad & E^Tx+\sum_{k=1}^{s}N_rp_kF^Ty_k\\ \text{s.t.}\quad & Ax\ge b,\\ & Gx+Ky_k+Lz_k\ge h,\\ & x\ge 0,\ y_k\ge 0,\ z_k\in\{0,1\} \end{aligned} \tag{45}$$

where x represents the vector of equipment capacity decisions in the upper-level configuration stage; y_k and z_k are the vectors of continuous and discrete operational variables under scenario k; E and F denote the coefficient vectors of the objective function.

The solution process of the Benders decomposition is illustrated in Figure 2.

Step 1: Model Initialization. Initialize the decision variables of the master problem x^0, and set the initial lower and upper bounds, the convergence tolerance ε, and the iteration counter $i=0$.

Step 2: Solve the Master Problem. In the i-th iteration, solve the master problem to obtain the current capacity configuration x^i and update the lower bound LB.

Step 3: Solve the Subproblem. Given the capacity configuration x^i, solve the subproblem to determine the operational scheduling strategy and corresponding operating cost, and evaluate its feasibility.

Step 4: Generate Benders Cuts. If the subproblem is infeasible, generate a feasibility cut to eliminate the infeasible capacity configuration. If the subproblem is feasible but not yet converged, generate an optimality cut to refine the LB of the master problem and update the upper bound.

Step 5: Convergence Check. If the convergence condition $|UB-LB|<\varepsilon$ is obeyed, terminate the iteration. Otherwise, set $i=i+1$ and return to Step 2.

Step 6: Output Results. Output the final optimal capacity configuration x^* and the corresponding operational scheduling strategy.

IV. CASE STUDY ANALYSIS

A. SYSTEM PARAMETER AND CASE SETTINGS

To verify the advantage of the bllevel model, a large rural area in Jiangsu Province is selected as the case study, and the analysis is conducted under the Python 3.9.13 environment. The service lifetime of each energy device in the system is set to 20 years, with a discount rate of 6%. The main investment parameters of the energy devices are listed in Table 1.

The PV power generation for the 12 typical days is shown in Figure 3.

Electric, thermal, gas, and hydrogen load power for typical days are shown in Figure 4.

To investigate the long-term characteristics of hydrogen energy storage, different scenarios are designed for verification.

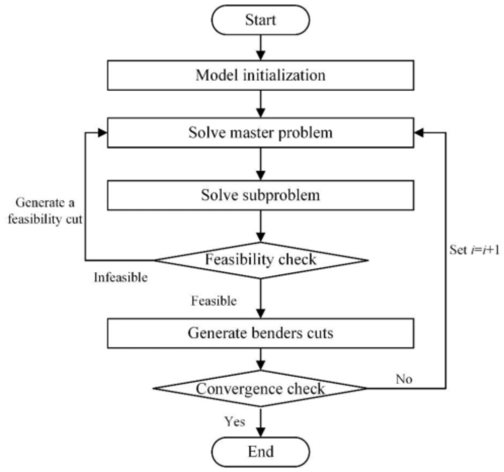

FIGURE 2. Benders decomposition–based solution process

TABLE I. Investment Parameters for Energy Equipment

Equipment	Investment cost	Rated capacity	Equipment	Investment cost	Rated capacity
Waste-to-power	29700¥/kW	6000 kW	CHP unit	15000¥/kW	1000 kW
Biogas fermentation	18000¥/kW	4000 kW	Battery	1000¥/kWh	20000 kWh
Electrolyzer	5000¥/kW	3000 kW	Thermal energy storage tank	200¥/kWh	20000 kWh
Hydrogen fuel cell	8000¥/kW	1000 kW	Hydrogen storage tank	3500¥/kg	2000 kg

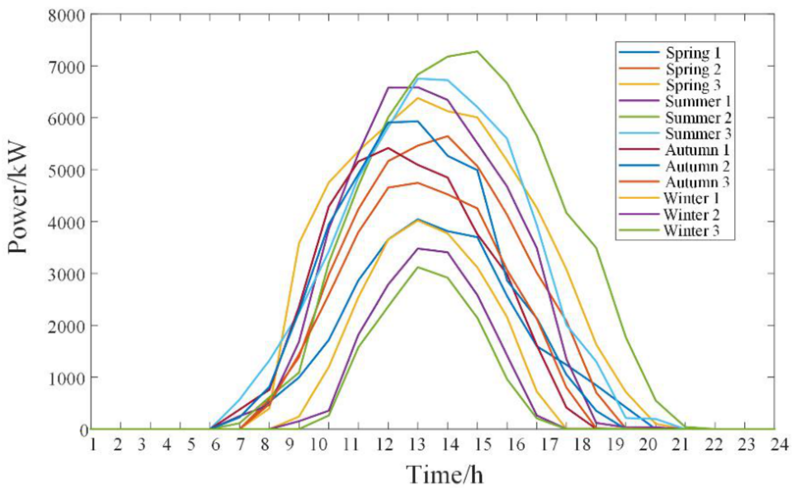

FIGURE 3. PV power output for typical days

Scenario 1: The daily energy variation of the hydrogen storage tank is constrained, considering only its short-term energy balance for system capacity configuration.
Scenario 2: The long-term operational characteristics of hydrogen storage tank are considered for system capacity configuration.

B. OPTIMIZATION CONFIGURATION RESULTS

The equipment capacity configuration results under different scenarios are shown in Table 2. Different hydrogen storage characteristics have a significant impact on system configuration. In Scenario 1, daily energy balance constraints on hydrogen storage limit cross-period regulation, leading to higher capacities of the electrolyzer, fuel cell, and battery to maintain short-term flexibility. In Scenario 2, the hydrogen storage tank enables long-term energy shifting, reducing the need for short-term devices and fossil-fueled units. As a result, system investment and operational dependence on conventional equipment are effectively reduced.

The results of the system life-cycle cost are shown in the Table 3. In Scenario 1, the total cost is slightly higher because the system requires more short-term flexi-

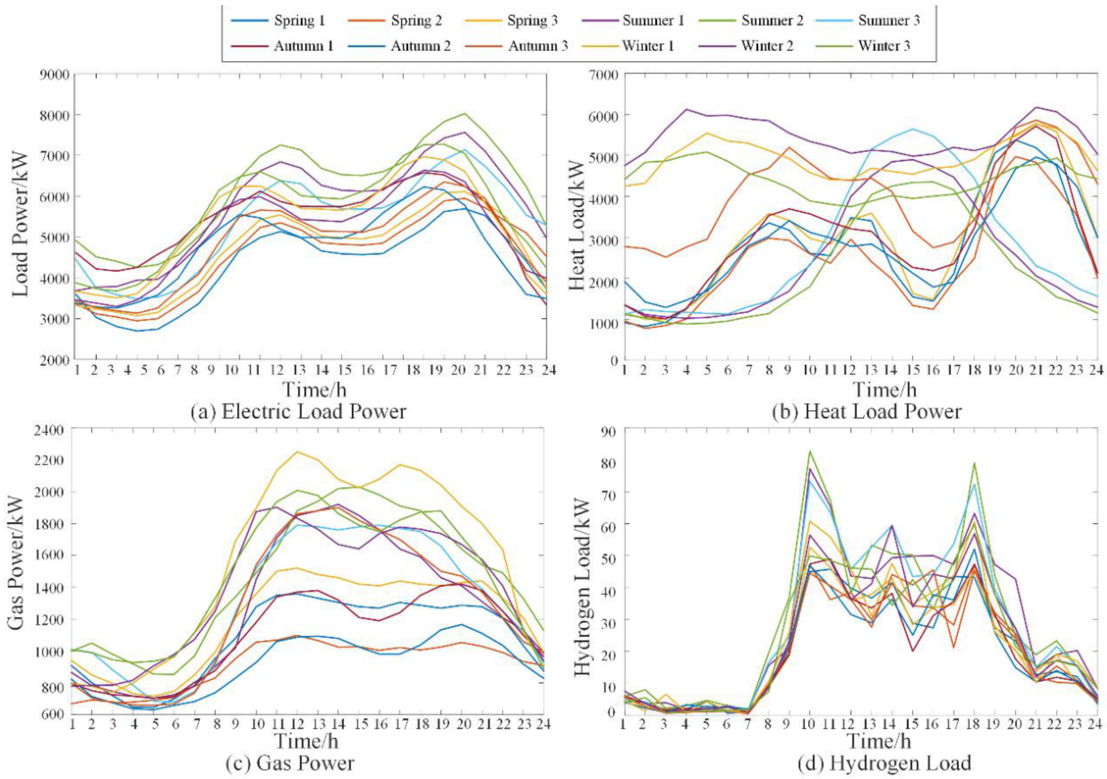

FIGURE 4. Electric, thermal, gas, and hydrogen load power for typical days

TABLE II. Equipment Capacity Configuration Results Under Different Scenarios

Scenario	Waste-to-power (kW)	Biogas fermentation (kW)	Electrolyzer (kW)	Hydrogen fuel cell (kW)	CHP unit (kW)	Battery (kWh)	Thermal energy storage (kWh)	Hydrogen storage tank (kg)
1	5608.55	1370.96	2973.97	132.02	247.78	20417.02	20257.10	254.34
2	5606.99	1438.52	2526.76	101.94	200.44	19489.04	20104.51	682.21

ble devices, leading to increased investment and operating costs. In Scenario 2, the total cost decreases. Although the hydrogen storage tank capacity increases significantly, the system mitigates redundant configurations of peak hydrogen production and power generation equipment through cross-period energy regulation, thereby reducing overall investment and loss costs.

As is shown in the Figure 5, the variation curves of hydrogen mass stored in the hydrogen tank over 8760 hours throughout the year under different scenarios.

C. OPTIMIZATION OPERATION RESULTS ANALYSIS

Under short-term operational constraints, the hydrogen storage tank only performs intraday regulation, resulting in low and stable hydrogen levels. The system mainly relies on short-term flexible devices such as electrolyzers, fuel cells, and batteries to maintain energy balance. When long-term operation is enabled, the hydrogen storage capacity and hydrogen level increase significantly, allowing long-duration energy shifting and optimized scheduling. The system achieves higher operational efficiency, improved storage utilization, and lower carbon emissions, leading to enhanced economic and low-carbon performance.

The electrical energy scheduling results for 12 typical days under different scenarios are shown in Figures 6 and 7. Under short-term constraints, the limited regulation capacity of hydrogen storage forces the system to rely more on purchased electricity to maintain energy balance, resulting in higher operating costs. When long-term hydrogen storage characteristics are considered, the system can achieve temporal energy shifting and optimized scheduling, significantly enhancing renewable energy utilization, reducing electricity purchases, and minimizing overall system costs.

TABLE III. System Life-Cycle Cost Under Different Scenarios

Scenario	Investment cost (10^6¥)	Operating cost (10^6¥)	Decommissioning cost (10^5¥)	Loss cost (10^4¥)	Total cost (10^6¥)
1	22.81	7.96	6.84	5.83	31.51
2	22.70	7.67	6.81	5.06	31.10

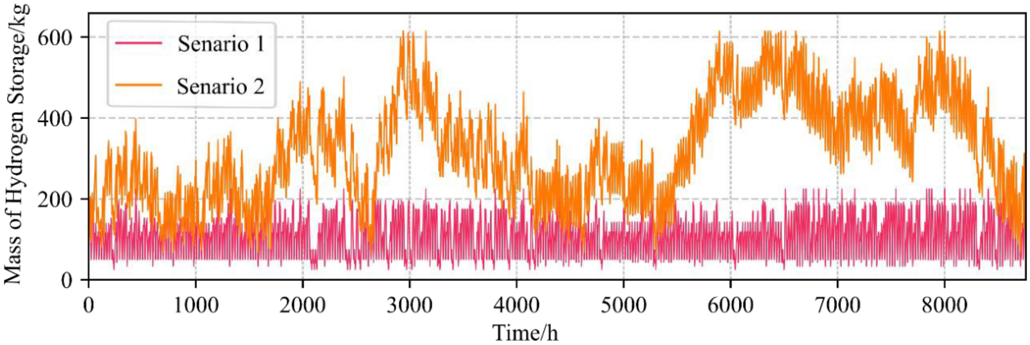

FIGURE 5. Hydrogen storage capacity variation curve

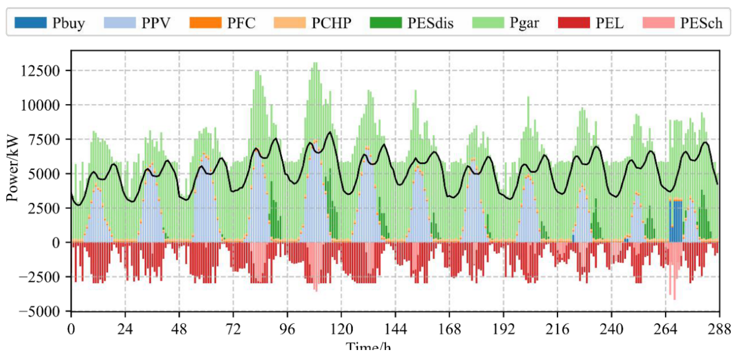

FIGURE 6. Electric energy flow curve in scenario 1

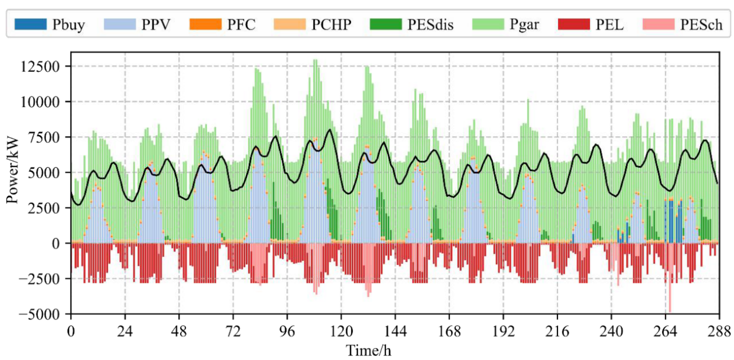

FIGURE 7. Electric energy flow curve in scenario 2

The thermal energy scheduling results for 12 typical days under different scenarios are shown in Figures 8 and 9, where the black line represents the thermal load of the system. Under short-term hydrogen storage conditions, waste-to-energy generation dominates the heat supply, and the CHP unit frequently cycles to match thermal load fluctuations. The limited regulation capacity of the thermal storage tank makes it difficult to smooth the heat supply. The biogas digester experiences significant thermal power fluctuations, which reduce gas yield and lead to low CHP stability, thereby limiting the overall thermal efficiency. During long-term hydrogen storage operation, waste heat from waste-to-energy and electrolyzers is effectively recovered, while the thermal storage tank and fuel cell coordinate heat release to achieve stable thermal power supply and efficient energy coupling. The biogas digester receives a more stable heat input, enhancing gas production. The system achieves higher thermal efficiency and lower carbon emissions, demonstrating the superior economic and low-carbon performance of integrated heat–electricity–hydrogen coordination.

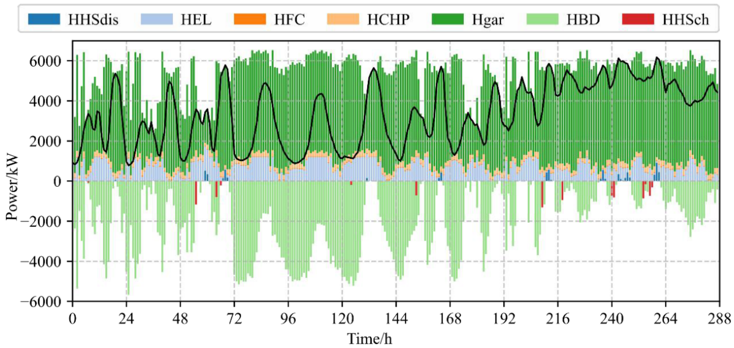

FIGURE 8. Thermal energy flow curve in scenario 1

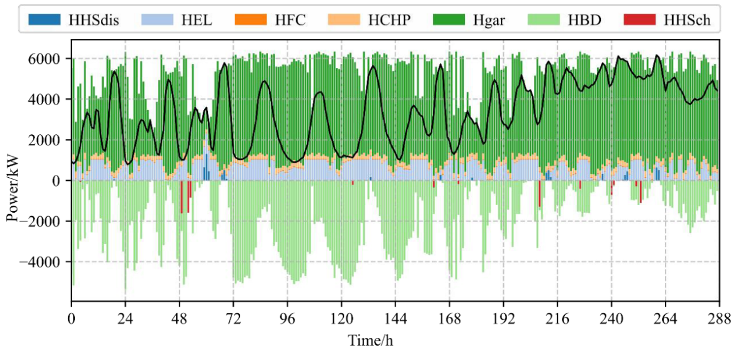

FIGURE 9. Thermal energy flow curve in scenario 2

The hydrogen energy scheduling results for 12 typical days under different scenarios are shown in Figures 10 and 11, where the black line represents the system hydrogen load. Under short-term storage conditions, hydrogen production is constrained, resulting in low and fluctuating storage levels, with limited conversion of surplus electricity. The system primarily maintains balance through hydrogen sales. With long-term storage operation, the hydrogen tank enables cross-period regulation, leading to increased hydrogen production and storage capacity. The system achieves flexible energy shifting and self-balancing, reducing external energy dependence and carbon emissions while improving both economic and low-carbon performance.

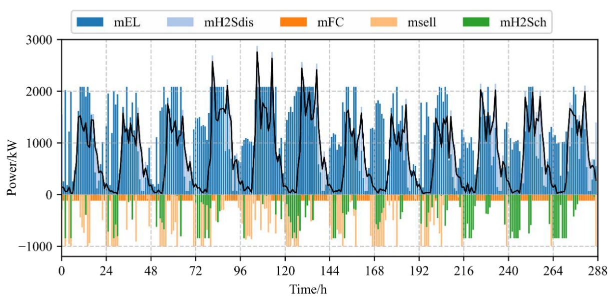

FIGURE 10. Hydrogen energy flow curve in scenario 1

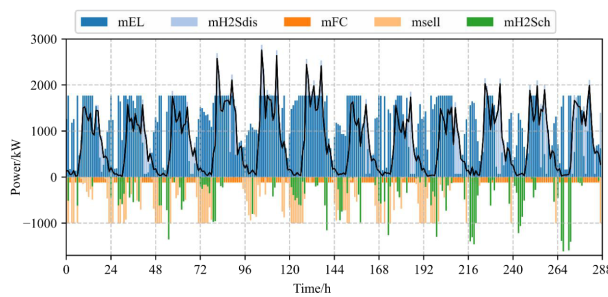

FIGURE 11. Hydrogen energy flow curve in scenario 2

TABLE IV. Operating Costs Under Different Scenarios

Scenario	Carbon emission (10^6 kg)	O&M cost (10^6¥)	Energy purchase cost (10^6¥)	Carbon trading cost (10^6¥)	Waste treatment subsidy (10^6¥)	Energy sales revenue (10^6¥)	Total operating cost (10^6¥)
1	8.03	8.90	1.17	2.22	1.52	2.81	7.96
2	7.87	8.98	1.01	1.99	1.53	2.78	7.67

Table 4 presents the system operating costs under different scenarios. Compared with short-term hydrogen storage, long-term hydrogen storage reduces the total system cost by approximately 3.6% and carbon emissions by about 1.9%, improving economic performance while achieving emission reduction.

By storing hydrogen during periods of PV surplus and releasing it in winter for power generation, the system effectively lowers energy purchase costs. Although hydrogen sales revenue slightly decreases, the overall operating cost and carbon emissions are reduced, demonstrating the dual advantages of long-term hydrogen storage in both economy and low-carbon performance.

V. CONCLUSION

This study focuses on the optimal configuration of electricity–hydrogen coupled systems considering the long-term characteristics of hydrogen storage. A bilevel optimization framework is proposed, and its effectiveness is verified through scenario-based comparative analysis. The main work and conclusions are as follows:

(1) A bilevel optimization model of the electricity–hydrogen coupled system is developed, with an upper-level capacity configuration model and a lower-level operational operating model. The upper level minimizes the annualized life-cycle cost to optimize equipment capacity, while the lower level minimizes the annual operating cost to determine the optimal dispatch strategy, achieving coordinated planning and operation.

(2) An efficient solution method based on Benders decomposition is proposed. Decomposing the original problem into a master problem and a subproblem, the global optimum is approached iteratively by generating feasibility and optimality cuts. This method effectively addresses the computational challenges of high-dimensional nonconvex problems, ensuring both convergence and efficiency.

(3) Comparative analysis of different hydrogen storage scenarios demonstrates the coordinated optimization benefits of long-term hydrogen storage. Compared with the short-term storage case, the total life-cycle cost decreases by 1.28%, the operating cost by 3.58%, and carbon emissions by 1.93%, indicating improved integration of planning and operational economy.

Future research will build upon the proposed configuration model to further investigate the real-time scheduling optimization of electricity–hydrogen coupled systems under economic stability constraints, aiming to achieve efficient coordination and dynamic operation across multiple time scales.

ACKNOWLEDGMENT

The authors acknowledge the Science and Technology Project of State Grid Jiangsu Electric Power Company (Grant: J2024187).

REFERENCES

[1] O. Alavi, I. Kaaya, R. De Jong, *et al.*, "Assessing the impact of PV panel climate-based degradation rates on inverter reliability in grid-connected solar energy systems," *Heliyon*, vol. 10, no. 3, Art. no. e25839, 2024.

[2] F. Dawood, M. Anda, and G. M. Shafiullah, "Hydrogen production for energy: An overview," *Int. J. Hydrogen Energy*, vol. 45, no. 7, pp. 3847–3869, 2020.

[3] A. Mohammadi and M. Mehrpooya, "A comprehensive review on coupling different types of electrolyzer to renewable energy sources," *Energy*, vol. 158, pp. 632–655, 2018.

[4] M. Shi, P. Xie, L. Yao, *et al.*, "Electricity-hydrogen coupled energy storage bilevel optimization for offshore wind-powered zero-carbon port microgrids considering multiple uncertainties," *Appl. Energy*, vol. 401, Art. no. 126672, 2025.

[5] X. Yu and G. Xu, "Optimized configuration of integrated energy system for parks with hydrogen storage and electric heat storage," *Power Demand Side Manage.*, vol. 26, no. 6, pp. 30–36, 2024.

[6] Y. Xiong, Y. Si, T. Zheng, *et al.*, "Optimal configuration of hydrogen storage in industrial park integrated energy system based on Stackelberg game," *Trans. China Electrotech. Soc.*, vol. 36, no. 3, pp. 507–516, 2021.

[7] G. Pan, W. Gu, H. Qiu, *et al.*, "Bi-level mixed-integer planning for electricity-hydrogen integrated energy system considering levelized cost of hydrogen," *Appl. Energy*, vol. 270, Art. no. 115176, 2020.

[8] N. Liu, K. Zhang, and K. Zhang, "Coordinated configuration of hybrid energy storage for electricity-hydrogen integrated energy system," *J. Energy Storage*, vol. 95, Art. no. 112590, 2024.

[9] S. Zhu, B. Du, X. Lu, *et al.*, "Design and optimization of a cascade hydrogen storage system for integrated energy utilization," *J. Energy Storage*, vol. 96, Art. no. 112732, 2024.

[10] M. Laimon and T. Yusaf, "Towards energy freedom: Exploring sustainable solutions for energy independence and self-sufficiency using integrated renewable energy-driven hydrogen system," *Renew. Energy*, vol. 222, Art. no. 119948, 2024.

[11] J. Park, S. Kang, S. Kim, *et al.*, "Optimizing green hydrogen systems: Balancing economic viability and reliability in the face of supply-demand volatility," *Appl. Energy*, vol. 368, Art. no. 123492, 2024.

[12] Z. Sun, Q. Ai, A. Julaiti, *et al.*, "Annual planning study of integrated energy system considering seasonal hydrogen storage and futures carbon trading," *Electric Power*, vol. 55, no. 8, pp. 2–13, 2022.

[13] M. Liu, G. Zeng, P. Dong, *et al.*, "Bi-level robust stochastic optimal configuration method for hydrogen energy storage system," *J. South China Univ. Technol. (Nat. Sci. Ed.)*, vol. 52, no. 9, pp. 12–23, 2024.

[14] X. Gao, X. Wang, L. Zheng, *et al.*, "Techno-economic optimization of a coupled electricity-heat-hydrogen energy system considering seasonal hydrogen storage and demand response," *Int. J. Hydrogen Energy*, vol. 180, Art. no. 151642, 2025.

[15] Y. Zhu and Q. Geng, "Capacity allocation and operation optimization of integrated energy park system coupled with hydrogen energy storage," *Modern Electric Power*, vol. 40, no. 6, pp. 931–938, 2023.

[16] L. Sun, L. Chen, Y. Xiong, *et al.*, "Capacity optimization configuration of hydrogen energy storage cogeneration integrated energy system considering photothermal collector module," *Electric Power Autom. Equip.*, vol. 43, no. 12, pp. 70–76, 2023.

[17] Y. Chen, L. Feng, I. Mansir, *et al.*, "A new coupled energy system consisting of fuel cell, solar thermal collector, and organic Rankine cycle; Generation and storing of electrical energy," *Sustain. Cities Soc.*, vol. 81, Art. no. 103824, 2022.

[18] Y. Cheng, *Research on Operation Optimization and Optimal Configuration of Hydrogen Energy Storage in Integrated Energy Systems with Hydrogen Production from Wind Power*. South China Univ. Technol., 2021.

[19] K. Zhang, *Optimal Capacity Allocation of Wind-Solar-Hydrogen Storage Integrated Energy System Based on Energy Storage Control Strategy and Improved NSGA-II Algorithm*. Ningxia Univ., 2019.

[20] R. Li, X. Peng, H. Lv, *et al.*, "Two-layer optimal configuration for integrated energy system regarding hydrogen storage and demand response," *J. North China Electric Power Univ. (Nat. Sci. Ed.)*, vol. 51, no. 1, pp. 74–82, 111, 2024.

[21] L. Sun, Z. Lin, and W. Li, "Research on multi-objective comprehensive energy optimization configuration scheme considering hydrogen storage," *High Voltage Apparatus*, vol. 60, no. 7, pp. 88–96, 2024.

[22] L. Lin, K. Ou, Q. Lin, *et al.*, "Two-stage multi-strategy decision-making framework for capacity configuration optimization of grid-connected PV/battery/hydrogen integrated energy system," *J. Energy Storage*, vol. 97, Art. no. 112862, 2024.

[23] G. Wang, K. Verleysen, M. De, *et al.*, "Multi-objective optimization of hybrid energy storage systems under uncertainty," *J. Energy Storage*, vol. 111, Art. no. 115218, 2025.

[24] A. Miao, Y. Yuan, Y. Huang, *et al.*, "Stochastic optimization model of capacity configuration for integrated energy production system considering source-load uncertainty," *Sustainability*, vol. 15, no. 19, Art. no. 14247, 2023.

[25] Z. Xu, F. Chen, X. Yang, *et al.*, "Optimal configuration of hybrid energy storage capacity in a grid-connected microgrid considering laddering carbon trading and demand response," *Energies*, vol. 17, no. 1, Art. no. 139, 2024.